

Insight into the Binding Mechanisms of Quartz-Selective Peptides: Toward Greener Flotation Processes

Abolfazl Alizadeh Sahraei, Barbara Mejia Bohorquez, Denise Tremblay, Sylvain Moineau, Alain Garnier, Faïçal Larachi,* and Patrick Lagüe*

Cite This: *ACS Appl. Mater. Interfaces* 2023, 15, 17922–17937

Read Online

ACCESS |

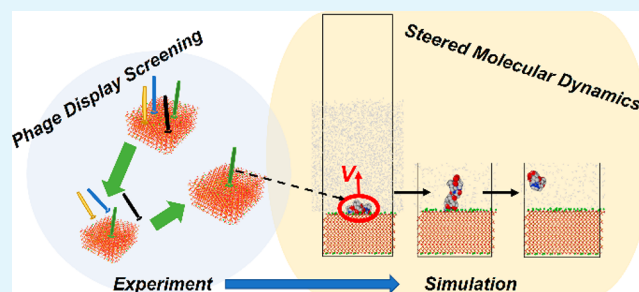
Metrics & More

Article Recommendations

Supporting Information

ABSTRACT: Mining practices, chiefly froth flotation, are being critically reassessed to replace their use of biohazardous chemical reagents in favor of biofriendly alternatives as a path toward green processes. In this regard, this study aimed at evaluating the interactions of peptides, as potential floatation collectors, with quartz using phage display and molecular dynamics (MD) simulations. Quartz-selective peptide sequences were initially identified by phage display at pH = 9 and further modeled by a robust simulation scheme combining classical MD, replica exchange MD, and steered MD calculations. Our residue-specific analyses of the peptides revealed that positively charged arginine and lysine residues were favorably attracted by the quartz surface at basic pH. The negatively charged residues at pH 9 (i.e., aspartic acid and glutamic acid) further showed affinity toward the quartz surface through electrostatic interactions with the positively charged surface-bound Na^+ ions. The best-binding heptapeptide combinations, however, contained both positively and negatively charged residues in their composition. The flexibility of peptide chains was also shown to directly affect the adsorption behavior of the peptide. While attractive intrapeptide interactions were dominated by a weak peptide–quartz binding, the repulsive self-interactions in the peptides improved the binding propensity to the quartz surface. Our results showed that MD simulations are fully capable of revealing mechanistic details of peptide adsorption to inorganic surfaces and are an invaluable tool to accelerate the rational design of peptide sequences for mineral processing applications.

KEYWORDS: molecular dynamics, SMD, REMD, phage display, quartz, peptides, rational design, floatation



1. INTRODUCTION

The ever-growing demand for mineral commodities has acutely grown the level of mineral beneficiation activities over the past decade. Traditional mining processes have shown their technical limits in terms of preserving the biosphere and, ultimately, living beings.^{1,2} Their disadvantageous consequences require a transition to greener solutions such as biofriendly and sustainable alternative reagents.³

Silica is one of the most abundant families of inorganic materials in the Earth's crust with applications in separation,^{4,5} biomedical materials,⁶ drug delivery,⁷ catalyst support,⁸ CO_2 storage/utilization,^{9,10} electromagnetic devices,^{11,12} and composite fillers.^{13,14} Silica is commonly found in nature mixed with other valuable minerals that are targeted for extraction. The concentration of the target metal-bearing minerals is generally processed by froth flotation,¹⁵ while silicates are usually categorized as gangue minerals. More recently, reverse flotation processes, separating gangue from metal-bearing ores by quartz flotation, have been widely employed in industrial applications to produce high-grade concentrates.^{16,17}

The overall separation efficiency in froth flotation is controlled with various reagents acting as collectors and/or

depressants. Collectors are amphiphilic reagents, consisting of a polar head with a selective affinity to the target mineral surface and a nonpolar (often) aliphatic chain whose role is to attach to the rising bubbles. Many of today's synthetically produced reagents³ are problematic in terms of environmental acceptability,³ and their replacement for greener flotation practices has become imperative. In this context, there has been a recent surge of research toward exploiting the potential of biomolecules, chiefly amino acids and peptides, as alternatives.^{18–23} Developing new biobased alternatives will depend on how well one can distinguish peptides according to their selective binding to specific minerals. A failure to understand the peptide–inorganic interactions would fundamentally limit progress in the rational design of the peptide chains that are optimized for each technological application.

Received: January 27, 2023

Accepted: March 16, 2023

Published: April 3, 2023



Phage display (also known as biopanning) is a combinatorial experimental approach to identify affinity-selected peptides for many materials, including inorganic compounds (e.g., silica family).^{24,25} In this technique, a library of a billion phage particles, each bearing a unique short peptide, is incubated with a specific target, and the most promising binding peptides can be identified by sequencing after several rounds of screening and enrichment.²⁶ While phage display offers false-positive, target-unrelated peptides (TUPs) may be detected due to the propagation of phages bound to nontarget substrates (e.g., plastic, albumin, and biotin) involved during the technique.²⁷ Of interest, next-generation sequencing techniques²⁸ coupled with bioinformatics tools^{29,30} can notably reduce the number of false positives. Still, the limitation of current laboratory instrumentation at the scale of 1 to 100 nm hampers direct insights into the surface environment, dynamic process, and binding mechanisms. This is where complementary guidance from molecular modeling becomes beneficial.

Computational methods, from quantum scale to microscale, are the tools of choice to shed light on phenomena at scales inaccessible experimentally and accelerate rational material design. Because of the continuous progress in high-performance computing (HPC) facilities and the maturity of state-of-the-art force fields, molecular dynamics (MD) simulations are increasingly playing a significant role in interpreting experimental data, understanding the dominant mechanisms, and accelerating transformative property predictions.^{31–41} In MD simulations, the reliability of the knowledge obtained is also based on the justification of the molecular models in relation to the experimental conditions; e.g., here, adsorbent surfaces should be modeled with scrutiny to be similar to the experimental environment. In the case of the silica family, for example, pH, ionic strength, surface type, density, and degree of ionization of silanol groups in the solution are critical factors that need to be included in the models.^{32–34,36,41}

MD simulations of peptide-containing systems pose technical difficulties due to the high probability of getting trapped in local minima within the simulation time scale.^{42,43} To overcome the issue, enhanced sampling techniques, particularly replica exchange molecular dynamics (REMD), were developed to improve the sampling of configurational space of the peptides and approach toward the global minimum.^{44,45} For instance, Sampath and Pfaendtner⁴⁶ employed MD in tandem with REMD simulations to study the binding properties of an amphiphilic 14-mer peptide on the amorphous and crystalline silica surfaces with identical chemistries and charge states. Comparing the free energy profiles revealed that peptide–surface binding is controlled by the interfacially adsorbed water layer; the denser the hydration layer, the weaker the peptide binding to the surface.

In recent years, notable studies have applied MD theories to identify amino acids and peptide sequences with strong binding affinities toward silica surfaces.^{31–36,41} In flotation applications, however, molecular modeling studies are rare for silicate systems and are limited to some emblematic cationic and anionic collectors.^{47–50} Notman et al.³¹ suggested that the local stiffness of a peptide chain, arising from the presence of proline residue, increases peptide adhesions to the quartz surface. The localized rigid regions in the amino acid sequence restricted the degree of self-interactions of peptides, which favorably prevented the occurrence of folded conformations in the system. Patwardhan et al.³² investigated the interactions of different peptide combinations on silica surfaces. The results demonstrated that

negatively charged silica surfaces favorably attract positively charged peptides by the ion-pairing mechanism through N-terminal, lysine, and arginine residues with surface siloxide groups. Hydrogen bondings of polar groups in the peptide side chains with the silanol and siloxide groups on the surface were also predicted to have a role in the bonding mechanism. Ramakrishnan et al.³⁵ assessed the molecular mechanism underlying the strong binding of three 12-mer peptides to silicon that were identified by phage display. Further mutation analysis indicated that threonine and tryptophan played vital roles in the affinity of a peptide toward silica surface. Moreover, the presence of sulfur-containing residue (methionine and cysteine) in the sequence largely contributed to the peptide–silicon interactions. Emami et al.³⁴ reported that negative charge density on the silica surface in the basic pH range made positively charged peptides more favorable for surface adsorptions. In this case, the efficiency of hydrogen bonds, hydrophobic interactions, and the attraction of negatively charged peptides are diminished.

In this study, we used phage display screening and MD simulations to scale the adsorption of short peptides with selective affinities toward quartz surfaces. Our primary interest is to scrutinize the useability of peptides as environmentally friendly alternative flotation collectors. Therefore, the experimentations and simulations are implemented at pH 9 to mimic some important base-metal flotation processes.⁵¹ Here, we focused on the hydrophilic peptide subsection with affinities toward the quartz surface. Quartz-binding peptides were selected at pH 9, identified by next-generation sequencing technology, followed by checking the scanner and reporter of target-unrelated peptides (SAROTUP) database for possible TUP motifs.^{29,30,52} MD simulations were then employed to model the binding characteristics of the selected peptide candidates to the quartz surface. Because estimating peptide-binding strength toward quartz surfaces was challenging due to the high degree of freedom of the overall system and the complexity of surface speciations,^{42,43} a sequential simulation procedure combining MD, REMD, and steered molecular dynamics (SMD) simulations was implemented to quantify the descriptions of peptide–surface recognition and binding characteristics.^{53,54}

2. PHAGE DISPLAY SCREENING

2.1. Biopanning Experiments. Crystalline quartz particles with a particle size of $+75\ \mu\text{m}$ were obtained from the COREM research center. One heptapeptide phage display library (Ph.D.-7 Phage Display Peptide Library Kit, diversity 1×10^9 sequences, New England Biolabs, NEB) was used for three rounds of biopanning experiments according to the manufacturer's protocol.⁵⁵ For the first round, 75 mg of ore was incubated with the heptapeptide library diluted in 1 mL of TBS (50 mM Tris-HCl, pH 9.0, 150 mM NaCl) + 0.1% v/v Tween 20 for 1 h. Incubation was followed by 10 washes with 1 mL of TBST (0.1% Tween-20 in TBS) to remove nonbinding phages, and phages were eluted with 1 mL of elution buffer (0.2 M glycine-HCl, pH 2.2). The eluate was transferred to a microcentrifuge tube and neutralized with 150 μL of neutralization buffer (1 M Tris, pH 9.2). For the second and third rounds of biopanning, the ore quantity was decreased to 25 mg, and the Tween concentration was raised to 0.3% and 0.5% to increase stringency during panning. Following each round of biopanning, the number of eluted phages was determined by titration and further amplified by infection of a mid log phase *Escherichia coli* ER2738. As

controls, the wild-type library was sequenced before panning, and one round of panning was made on polypropylene (plastic) tubes.

2.2. Illumina Sequencing. After each round of biopanning and phage amplification, one part of the library was used for the next selection round, and the remaining library was used for sequencing. DNA extraction was made as described by NEB.⁵⁵ One step of purification with phenol:chloroform was performed according to Matochko et al.⁵⁶ The desired DNA region was amplified and equipped with the linkers necessary for Illumina sequencing. The forward primer used was 5'-TCGTCGGCAGCGTCAGATGTGTATAAGAGACAGTGGTTG-TTGTTCATTGTCGG-3', and the reverse primer was 5'-GTCTCGTGGGCTCGGAGATGTGTATAAGAGACAGG-TAGCATTCCACAGACAGCC-3'. The PCR was performed by 30 cycles of incubation and amplification. After this PCR step, the 16S Metagenomic Sequencing Library Preparation (Part # 15044223 Rev. B) protocol by Illumina was followed starting at the first Clean-UP step. Deep sequencing was performed on instrument MiSeq using the MiSeq reagent KitV2 following the protocol proposed by Illumina.⁵⁷ Demultiplexing of data, as well as the sequencing translation, was performed by a customized Python script.

2.3. Phage Display Screening Results. Table 1 shows the results after each round of panning on quartz and the controls of

Table 1. Overview of the Phage Display Sequencing Results at pH = 9

mineral	round	Tween concn (%)	total number of sequences	unique sequences
quartz	1	0.1	114224	98 937
	2	0.3	136930	15 902
	3	0.5	141428	5338
empty tube (polypropylene)	1	0.1	70702	2327
wild-type library	0	0.0	124214	122 226

the experiment (polypropylene and the wild-type library). Each peptide frequency was normalized by the total number of sequences in each library. The third round of panning on quartz was compared with the polypropylene and wild-type library, and the peptides found after the third panning on quartz and at very low frequency in the polypropylene library were selected as peptide candidates. These candidates were further analyzed

using the SAROTUP web server, and those peptides with a low probability of being nonspecific peptides were selected. The hydrophobicity of the peptide candidates was also calculated using the KyteDoolittle scale.⁵⁸ The final peptide list and its characteristics are summarized in Table 2.

3. SIMULATION METHODOLOGY

3.1. Peptide Models. The combinatorial phage display method was used to identify strongly binding heptapeptides on the quartz surface at pH 9 (Section 2). The experimental screening addressed the adsorption of ten 7-mer peptides with an affinity toward the quartz surface (Table 2). The zwitterionic forms of the ten candidates, considering their protonation state adjusted to pH 9, were prepared using the Avogadro code^{59,60} (see Figure S1 for the elongated conformation of the peptides). At pH 9, the peptides KPLVAQI and QFNHPKG bear a net charge of +1, while TDRDSTT and WSLDPSS carry a net charge of -1, and the rest are neutral. The excess charges of amino acid sequences K⁺, R⁺, D⁻, and E⁻ in the peptide were neutralized by Cl⁻ and Na⁺ counterions.

A scenario based on the replica exchange molecular dynamics (REMD) was introduced to investigate the adsorption behavior of peptides on the quartz surface. REMD, also known as *parallel tempering*, mainly applies to systems with rough energy landscapes.^{44,45} The general idea was to simulate several replicas of the same system parallelly at different temperatures while allowing the system to exchange complete configurations between the adjacent temperature replicas. More efficiently, instead of passively waiting for the occurrence of rare spontaneous incidents, REMD lets the higher temperatures overcome energetic barriers and obviate the sampling problem associated with the presence of multiple minima.

We employed REMD within the first two steps of the simulation pathway. An elongated conformation of the peptide was first built (Figure S2a) and then placed in a box of 49.1 × 51.1 × 80 Å³ dimensions. Following the energy minimization by the conjugate gradient method for a maximum of 10⁵ steps, the first REMD simulation was conducted in the implicit water environment. We preferred the implicit water model over the explicit one because this initial sampling would act as a transient conformation; therefore, extra computational efforts are not expected to lead to remarkable differences in the final quartz/peptide/water configurations. Eight replicas, distributed exponentially within the temperature range of 300–500 K, were

Table 2. Sequence and Properties of 10 Peptides Exhibiting High Affinity toward Quartz Surface at pH = 9 Obtained by the Phage Display Technique

peptide	GRAVY ^a index	charge at pH 9.0	polystyrene surface binding probability	Mimo Scan hits ^b	Mimo Search hits ^b	Mimo Blast hits ^b
FTPDGAR	-0.87	0	0.08	NO	NO	NO
HPVYPQA	-0.74	0	0.23	NO	NO	NO
KPLTADL	-0.04	0	0.02	NO	NO	NO
KPLVAQI	0.76	+1	0.06	NO	NO	NO
KQPIPEL	-0.83	0	0.42	NO	NO	NO
MDMNGKY	-1.26	0	0.19	NO	NO	NO
QFNHPKG	-1.90	+1	0.15	NO	NO	NO
TAWASAA	0.68	0	0.42	NO	NO	NO
TDRDSST	-2.06	-1	0.03	NO	NO	NO
WSLDPSS	-0.66	-1	0.46	NO	NO	NO

^aGRAVY index: a negative score means that a peptide is hydrophilic, while a positive score means that a peptide is more hydrophobic. ^bMimo Scan, Mimo Search, and Mimo Blast are tools based on database search in the biopanning databank (BDB) to find identical or similar peptides to the query peptide.

selected for the REMD simulations. The exponential temperature distribution usually leads to a uniform acceptance ratio assuming a constant heat capacity over the intervals.^{61,62} The time step was set to 2 fs, and exchanges between replicas were attempted every 1 ps. The simulations continued under the NVT ensemble for 50 ns. The equilibration of the isolated implicit water solvated peptide system was identified by monitoring the variation of temperature, center of mass (COM), radius of gyration, and solvent-accessible surface area (SASA). The final snapshot of the peptide conformation at the lowest temperature ($T = 300$ K) was recorded for the next step (Figure S2b). Sampling with REMD, two initial conformations, elongated and replica exchanged for each peptide, were chosen to construct the initial complex peptide–quartz system configurations. For brevity, hereafter, we included “*El*” and “*RE*” abbreviations into the sample names to denote the configurations obtained by initially placing elongated and replica exchanged peptides on the surface, respectively.

3.2. Quartz Slab Model. Realistic model reproduction of a surface is crucial for thoughtful simulations of the inorganic–biomolecular interfaces. In this regard, the Nanomaterial Modeler tool of CHARMM-GUI (<https://charmm-gui.org>) was employed to build the silica slab.⁴¹ The crystalline quartz surface was created by cleaving its unit cell in the (001) direction, expanding in 3D to construct a $49.1 \times 51.1 \times 28 \text{ \AA}^3$ slab supercell, and finally saturating the superficial Si atoms by silanol groups with a density of 9.4 groups/nm². These assumptions led to the Q² species surface, i.e., the (Si–O)₂Si(OH)₂ chemical environment consisting of two silanol groups per each superficial Si atom.^{32–34} Along with the substrate type determining the area density of silanol groups on a silica surface, the precise silanol ionization degree (i.e., the deprotonation of silanol group to sodium siloxide with the (Si–O)₂Si(OH)(–O[–]...Na⁺) formulation) should always be considered in the model construction.³³ In the case of the silica family, the ionization degree is a function of the solution pH and substrate type and should be ascertained by either referring to reliable literature or direct experimental measurements.³³ At the working pH of 9, the fraction of silanol groups ionized to sodium siloxide has been reported to be 20% for the quartz surface with the Q² environment.^{32–34} The final quartz surface model employed in the course of simulations is presented in Figure S3.

3.3. Simulation Details. All simulations used the interface force field (IFF) for quartz,^{33,34,41} CHARMM36 for peptides and ions,⁶³ and TIP3P for the explicit water model.⁶⁴ Simulations were performed with LAMMPS (Large-scale Atomic/Molecular Massively Parallel Simulator), an open-source code distributed by Sandia National Laboratories,⁶⁵ and visualizations were processed by OVITO (The Open Visualization Tool).⁶⁶

In the subsequent course of simulations, the REMD method was further utilized to sample the surface–peptide interactions using the *El* and *RE* peptide conformations obtained from the previous step. To do so, conformers were placed at an $\sim 5 \text{ \AA}$ distance from the quartz surface (Figure S2c), and each system independently underwent REMD calculations in an implicit water environment in the presence of the slab. To reduce the computational cost, only silanol and sodium siloxide groups of the quartz slab were free to move during the simulations. The REMD simulations were conducted for 25 ns while the other parameters were the same as in the previous step. The system snapshots, temperature, energy, the center of mass (COM) of the peptide, and its gyration radius were recorded per replica

every 2 ps to monitor the convergence of the simulations (see Figure S4 for sample outputs). Trajectories at $T = 300$ K were also reordered in a single LAMMPS dump file for further conformation analysis (see Figures S5 and S6). Ultimately, the final adsorption configurations at $T = 300$ K (Figure S2d) were taken to the next step.

The next step was to introduce explicit water molecules to the preadsorbed peptides on the surface. In this regard, 6600 water molecules were placed in a 3D periodic box of $120 \times 120 \times 120 \text{ \AA}^3$, followed by an isotropic NPT at 300 K and 1 bar for 1 ns to find its equilibrium density. For a feasible merging with the quartz–peptide slab, the x – y dimensions of the water box were adjusted to the quartz surface area, and then after, the simulation continued for 1 more ns under an NVT ensemble. The well-equilibrated water box was then placed at a $\sim 3 \text{ \AA}$ distance on the quartz–peptide interface model, as shown in Figure S2e. The model obtained underwent a short NVT simulation of 0.5 ns to solvate both the peptide and the quartz surface. A moving Lennard-Jones (LJ) wall was also employed to push the water molecules toward the surface to ensure water–surface encounters (see Figure S2e). The slab and peptide atoms were kept rigid throughout the water solvation process to prevent system collapse. The final quartz–peptide–water model included the quartz slab, peptide–solution region ($\sim 80 \text{ \AA}$ in thickness), and a vacuum (of $\sim 60 \text{ \AA}$) on the top, as presented in Figure S2f. The vacuum was set large enough, so the water molecules did not interact with the slab’s bottom surface. Moreover, incorporating the vacuum on the top headspace provided the condition for the vapor phase to be developed as the simulations progress effectively, enabling a liquid/vapor interface to form. An LJ wall was also defined on the cell’s upper edge to avoid escaping the possible evaporated water (i.e., those water molecules leaving the water–vacuum interface and forming gas-phase water) from the box and make the application of long-range electrostatic calculations possible. The thicknesses of the solution phase were also sufficient to ensure bulk-like behavior, as confirmed by the calculation of the density profile in the z -direction.

All-atom molecular dynamics simulations were employed to equilibrate the quartz–peptide–water systems in the NVT ensemble at 300 K with the Nosé–Hoover thermostat. At this stage, only the quartz slab, except the silanol and sodium siloxide groups, were assumed to be rigid. A nonperiodic boundary condition was applied along the z -direction to preserve the integrity of the liquid–gas interface. The velocity-Verlet algorithm, with an integration time step of 1 fs, was selected to integrate Newton’s equation of motion. A cutoff with inner and outer distances of 10 and 12 \AA was applied for the vdW interactions, and the long-range electrostatic interactions were treated by the PPPM method with an accuracy of 10^{-5} . The SHAKE algorithm was used to constrain all bonds involving hydrogen atoms.⁶⁷ The MD simulations for each peptide system consisted of a minimum equilibration time of 50 ns followed by a production run of 5 ns.

3.4. Steered Molecular Dynamics (SMD) Simulations. SMD was implemented to characterize the binding strength of the peptide to the quartz slab. For conducting the SMD simulations, the peptide COM was pulled out in the z -direction at a constant velocity of 10^{-6} \AA/fs . Throughout the SMD simulations, the temperature was kept fixed at 300 K under the NVT ensemble applying the Nosé–Hoover thermostat. The final snapshot of the equilibrium runs from the peptide–quartz–water simulations was used as the starting configuration for the

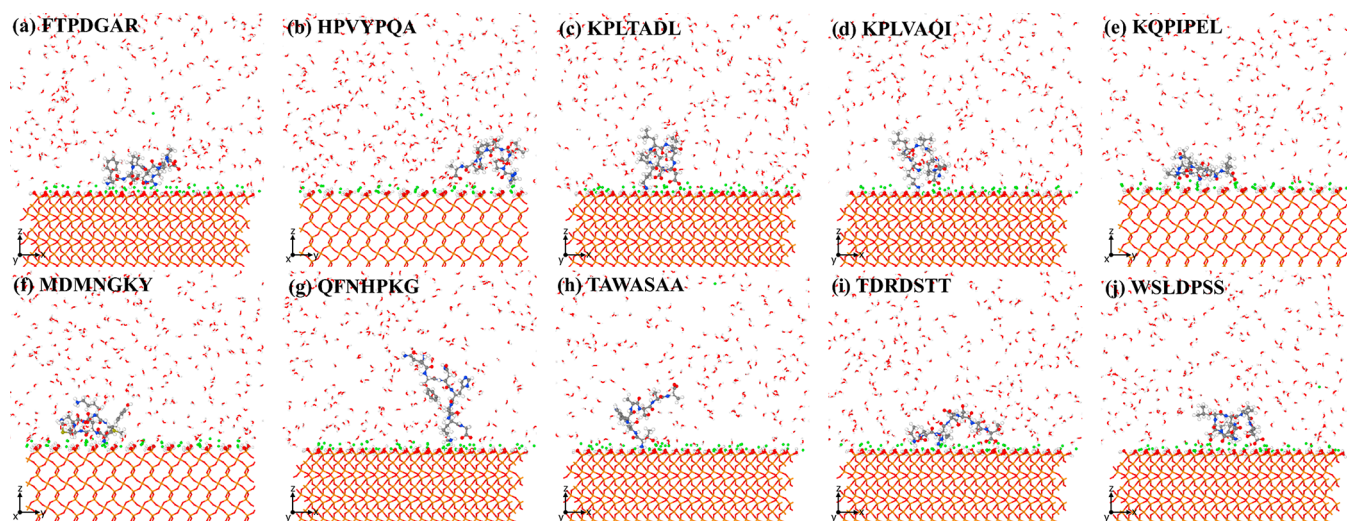


Figure 1. Selected equilibrated conformation of solvated (a) FTPDGAR, (b) HPVYPQA, (c) KPLTADL, (d) KPLVAQI, (e) KQPIPEL, (f) MDMNGKY, (g) QFNHPKG, (h) TAWASAA, (i) TDRDSTT, and (j) WSLDPSS peptides on quartz surface at pH = 9 at $t = 50$ ns ($H \equiv$ white, $C \equiv$ gray, $N \equiv$ blue, $O \equiv$ red, $S \equiv$ yellow, $Si \equiv$ orange, and $Na \equiv$ green). Note: the images are presented in the unwrap mode.

SMD simulations. The integration time step was set at 1 fs, similar to the equilibration phase. The pull-out simulation continued until the peptide's COM was at least 20 Å away from the surface. SMD simulations were repeated at least four times for each peptide adsorption model, initially obtained by the *El* and *RE* peptides on the slab. The PMF difference between the final state (i.e., detached peptide in solution) and the starting state (i.e., the adsorbed mode) was used to determine the relative order of affinity of peptides toward the surface. Analysis of SMD trajectories further elucidated the atomistic information about the binding/unbinding mechanism of the peptides under investigation.

4. RESULTS AND DISCUSSION

A rational modeling procedure was introduced to investigate peptide–mineral interactions in an aqueous environment. The proposed methodology consists of five modeling steps: (a) construction of experimentally consistent peptide–mineral models, (b) sampling of peptide–mineral interactions using an implicit water model and the replica exchange MD method, (c) introduction of explicit water to the obtained configurations, (d) equilibration of the mineral–peptide–water systems within the classical MD framework, and (e) quantifying peptides affinity and exploring phenomenological and mechanistic explanations of unbinding routes by SMD theory. Our calculations address the adsorption behavior and binding characteristics of 10 heptapeptides selected via phage display, showing selective binding to quartz surface (see Table 1 and Figure S1 for the list of candidates).

In this section, our primary focus is dedicated to characterizing the SMD simulations to unveil the binding free energies, the binding mechanism, and the origin of affinity differences of the solvated peptides. The variations of temperature, COM, gyration radius, SASA, interaction energies, and hydrogen bond evolution were monitored to assess the performance of REMD simulations and to determine if an equilibration state has been reached. The readers are invited to survey the Supporting Information for sample results.

4.1. Equilibration of the Mineral–Peptide–Water–Ion Systems. The final configurations of the peptides close to the quartz surface in the presence of explicit waters at pH 9 after 50

ns of MD simulations are depicted in Figure 1. The figure presents only one snapshot of the two sampling approaches (*El* or *RE*) for each peptide (i.e., the one with the higher affinity toward the quartz surface calculated through SMD simulations). Different view representations of the same snapshots can be found in Figure S7. Our observations revealed that for the weakest peptide–surface configurations, the peptides were detached from the surface in the first 20 ns of the trajectories.

Previous studies, in general, have captured ion-pairing, hydrogen bonds, hydrophobic interactions, and conformation effects as the central binding mechanisms that contribute to peptide–surface interplays.³² In this study, being in an aqueous environment at pH > pzc (i.e., point of zero charges is between 2 and 4 for quartz^{32,33}), alkali cations neutralized the negative surface charge and established an electric double layer composed of negatively charged siloxide groups and positively charged alkali ions. The electric double layer formation at the solid–liquid interface was a key feature in understanding interfacial chemistry though it complicates recognition of the dominant interaction mechanisms.⁶⁸

Within the amino acid sequences in the peptide candidates, *K* and *R* bear a charge of +1, *D* and *E* have a charge of −1, and the rest are neutral at pH = 9. As shown in Table 1, HPVYPQA and TAWASAA peptides are the two candidates with no charged amino acid sequences in their structure at pH 9.

Reviewing the snapshots alluded that almost all Na^+ cations remained bound to the surface during the equilibration runs, consistent with other reports.^{32,33} The final configurations in Figure 1 suggest that all the peptides screened by the phage display would bind to the quartz surface at pH = 9. However, the top-view snapshots (see the last column in Figure S7) revealed that the location of minimum-energy configuration on the quartz surface would differ per peptide sequence (the surface formulation was the same in all simulations). Moreover, while some candidates showed a tendency to fold in semiglobular configurations (e.g., KPLTADL, KPLVAQI, and WSLDPSS), some others rather extended their structures to align parallel to the surface and formed flat-on arrangements (e.g., FTPDGAR, KQPIPEL, MDMNGKY, and TDRDSTT). Further observations on the proximity of individual residues within the last 5 ns of equilibration trajectories demonstrated that hydrophobic side

groups have no (or minimal) affinity to the quartz at pH = 9 and position farther from the surface. This is due to the formation of the hydration shells of siloxide and Na⁺ cation on the ionized quartz slab, which keeps the hydrophobic residue away.³⁴ Our scrutiny on the trajectory files showed that the hydrophobic groups were positioned in the opposite direction from the surface. The negatively charged species mainly anchored to the surface by electrostatic bridging interactions with the surface-bound Na⁺ ions, while protonated amine groups were most specifically in contact with the siloxide groups through strong electrostatic interactions.

4.2. Steered Molecular Dynamics (SMD) Simulation

Results. SMD was utilized to gain insights into the binding strength of the peptide to the quartz slab through a nonequilibrium course of simulations. In SMD, the free energy profile of the peptide as a function of distance, also known as the potential of mean force (PMF), is extracted through Jarzynski's equality.^{69,70} The PMF profile provides qualitative and possibly quantitative correlation with the peptide–surface binding affinities.⁷⁰

To decipher the adsorption characteristics of the different peptides, SMD simulations were performed on each system, where the starting configurations were the final states of the equilibration stage. The corresponding PMF values as a function of distance of peptides were calculated during the SMD tests and are shown in Figure S8. As seen in the figure, two systems, namely HPVYPQA and MDMDGKY, contain only one set of foursome sampling. These peptides lost their bound state conditions within the equilibration simulations upon one of the initialization samplings.

The inflection points along the PMF–distance curves are indicative of different regimes during the detachment process associated with distinct molecular mechanistic processes. For relatively strong binding peptides (e.g., TDRDSTT and FTPDGAR), the PMF curves represented the following general stages: (1) initial perturbation from the stable surface adsorption configurations, (2) low-tension peptide extension in which weakly bound species were detached from the surface, (3) high-tension extension in which the peptides were stretched to the highest degree while the remaining bound groups are apart, and (4) dragging peptides through bulk solution indicated with the plateau in the PMF curves. For the relatively loose peptides (e.g., HPVYPQA, TAWASAA, and WSLDPSS), the debonding primarily lay in the first and (possibly) second regimes, and the chain extension vanished upon the separation. On the contrary, the existence of surface–philic amino acid sequences in the peptides fed the contribution of the high-extension regime, reflecting the higher peptide–surface interactions.

The distance the peptides were entirely out of the binding site (i.e., the distance at which the PMF curve became a plateau) also indicated the tendency of peptides for stretching upon detachment. The longer the separation distance, the higher the resistance of peptides to separation by forming extended conformations. As found in Figure S8, FTPDGAR, KPLVAQI, KQPIPEL, and TDRDSTT showed the highest separation distance of ~10 Å among all candidates.

The PMF difference between the beginning and the separate states was chosen to rank the affinity of peptides to the quartz surface. In this regard, the maximum of the average values per sampling was defined as the main criterion. The sorted peptides, from highest to lowest affinity, considering the PMF values, are illustrated in Figure 2. Based on the results, TDRDSTT,

FTPDGAR, and KQPIPEL were the three peptide candidates with the highest affinity toward quartz surfaces at pH = 9.

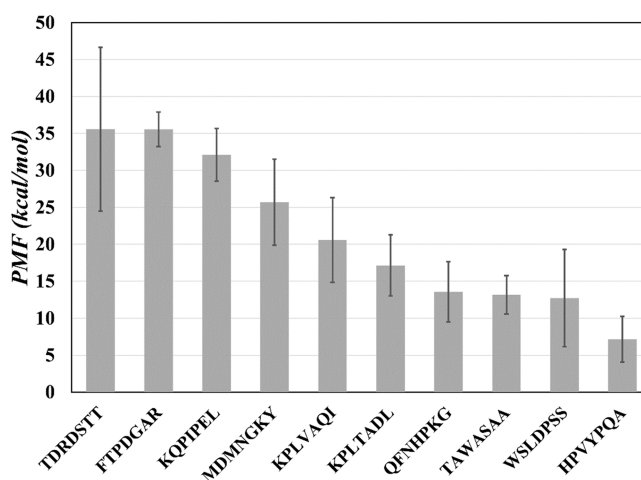


Figure 2. Binding characteristics of the solvated peptides on quartz surfaces at pH = 9 based on the PMF profiles obtained by the SMD simulations in Figure 3. The reported values for each peptide are the maximum of averaged PMF values per initialization conformations.

Interestingly, all the top three peptides contain at least one positively charged (i.e., arginine or lysine) and one negatively charged (i.e., aspartic acid or glutamic acid) amino acid sequence. This result was expected because the quartz surface contains silanol, sodium siloxide, and surface-bound Na⁺ counterions at basic pH. At pH = 9, the cationic groups with extra hydrogens interact with the surface through the salt bridging mechanism, i.e., hydrogen bonding with the oxygen-containing surface species or electrostatically by ion-pairing or ion exchange with the negatively charged siloxide groups.³² Meanwhile, for the anionic residues on the peptides, the surface-bound Na⁺ ions could electrostatically bridge the peptide connection to the surface. The deprotonated hydroxyl groups of aspartic acid (D⁻) and glutamic acid (E⁻) could also contribute to hydrogen bonding only as an acceptor. However, the latter case is less favorable due to the repulsive forces between these anionic residues and the negatively charged quartz surface. Consulting the equilibration images in Figures 1 and S7, the existence of oppositely charged species, especially D⁻ and R⁺, simultaneously in peptide structures resulted in a favorable elongated adsorption configuration upon equilibration.

HPVYPQA, WSLDPSS, TAWASAA, and QFNHPKG were rather weakly bound to the quartz surface at pH = 9, as seen in Figure 2. The PMF value of the least favorable peptide (i.e., HPVYPQA) was 5 times lower than the best candidates. Histidine with pK_a ≈ 6 is unchanged in the basic environment. As a result, HPVYPQA and TAWASAA were the only candidates with no charged residues in their structure. A solely charged amino acid sequence in WSLDPSS and QFNHPKG peptides also appeared to have a less efficient contribution to the peptide–quartz interactions. However, PMF differences in KPLVAQI and WSLDPSS peptides indicated that a positively charged residue (i.e., K⁺) was more favorable than a single negatively charged one (i.e., D⁻) for the quartz surface at basic pH. Yet, the importance of the residue's order and the neighboring amino acids in a sequence should not be neglected.

One should notice that the high occurrence of a peptide through phage display does not necessarily guarantee its higher

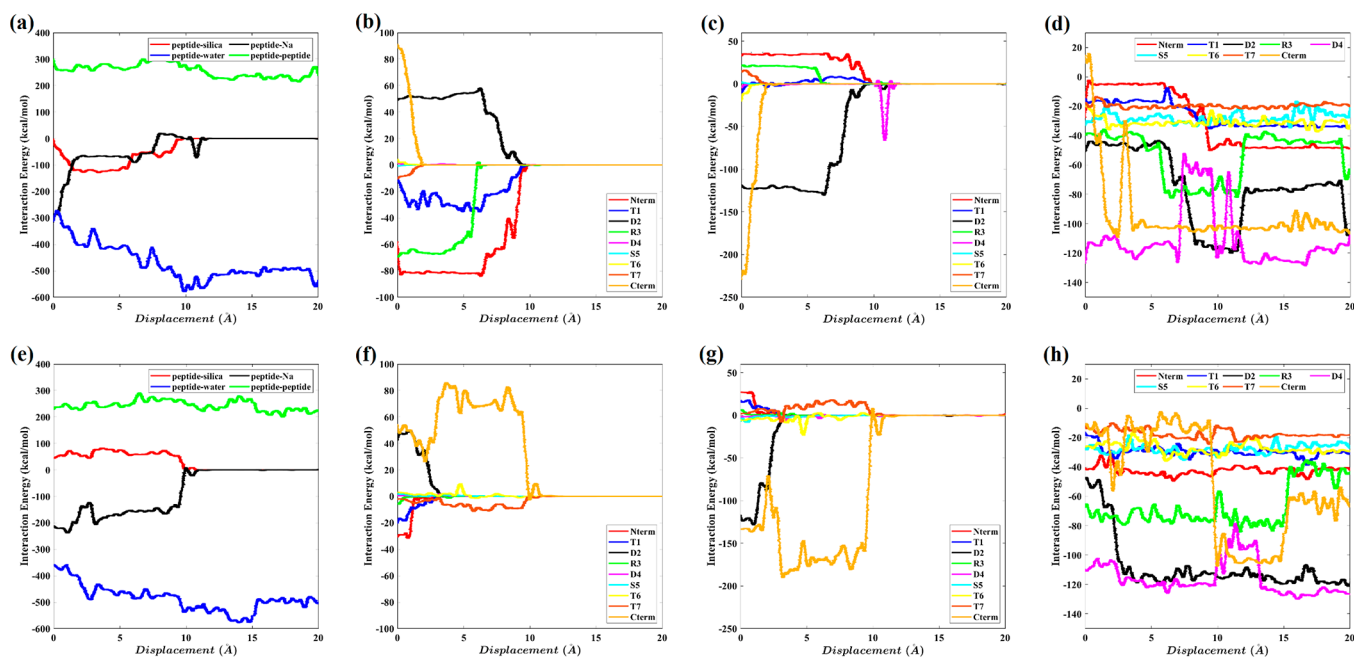


Figure 3. Evolution of the interaction energies during the pull-out process of solvated TDRDSTT (coded as T1D2R3D4S5T6T7 in the figures) from quartz surface at pH = 9 per elongated (upper row: panels a–d) and replica-exchanged (bottom row: panels e–h) initial conformations. (a, e) Overall variation of interaction energies. Contributions of each amino acid sequence in the interaction energies between (b, f) peptide–surface, (c, g) peptide– Na^+ counterions on the surface, and (d, h) peptide–water during peptide separation.

binding affinity toward the surface. As previously observed,^{35,71,72} thermodynamically unstable peptide sequences may have been overrepresented in the phage display process due to their high amplification rate rather than an actual surface-specific adhesion peptide.

4.3. SMD Trajectory Analyses. The analysis of trajectories during the SMD process provided valuable insight into adsorption/desorption mechanism of peptides. In this context, monitoring the interaction energies, close contact, and H-bonds is highly important. Here, we confine our survey to the most and minor binding candidates to clearly distinguish the underlying mechanisms.

4.3.1. TDRDSTT Peptide: Comparing *El* and *RE* Samplings.

The evolution of overall interaction energies and the respective contribution of amino acid sequences in the TDRDSTT (coded as T1D2R3D4S5T6T7 for clarification) system are shown in Figure 3. To clarify the difference in the sampling process, postprocessing was performed for both the elongated (*El*) and replica exchanged (*RE*) TDRDSTT initial conformations. The quartz surface, Na^+ counterions, peptide, and water molecules were treated as separate groups for energy calculations. The interaction energy (i.e., the sum of Coulombic and van der Waals (vdW) interactions) could be either negative or positive, indicating attraction or repulsion interplays, respectively. Comparing the overall interactions at a distance of zero in Figures 3a and 3e show that the two sampling procedures (i.e., *El* and *RE*) had converged to different conformations after equilibration. For the TDRDSTT–*El* sampling (Figure 3a), the peptide–quartz interaction was almost zero at the equilibrated state (i.e., at a distance of zero in the figures); however, the residue-specific calculations revealed that the N-terminus threonine (T1) and arginine (R3) had a considerable contribution to the peptide–surface interactions (Figure 3b). Closer observations (i.e., close contact analysis with surface siloxide groups, not shown here) ascertained that these cationic

groups were coordinated with negatively charged surface sites by forming ion pairs without exchanging surface-bound Na^+ ions. The C-terminus and the first aspartic acid (D2) residue in a row repelled from the surface and were attracted to the Na^+ ions positioned on the surface (Figure 3c). As stated earlier, Na^+ ions would keep the negatively charged residues near the surface by bridging the two homologous termini on the peptide and quartz surface.

In the case of TDRDSTT–*RE* sampling (Figure 3e), the peptide–surface interactions were positive during the pull-out process (before 10 Å displacement). Further observations in Figure 3f indicated that the contribution of N-terminus T1 in the *RE* sample was much lower than that in the *El* case, and R3 interactions had almost vanished. Thus, the conformation obtained in the TDRDSTT–*RE* prevented arginine residue from seeing the surface. Based on Figure 3g, the electrostatic interaction of $\text{O}^- - \text{Na}^+ - \text{O}^-$, where the first O^- belongs to the C-terminus and the second one is for the siloxide surface groups, was the primary adsorption mechanism in the TDRDSTT–*RE* system.

Monitoring the development of interaction energies during SMD provided information about the mechanism of peptide detachment. The detachment in the TDRDSTT–*El* system started from C-terminus T7 and was followed by R3 detachment around 6 Å (Figures 3bc and S9). The N-terminus side, including the two neighboring T1 and D2 residues, were the strongest sequences resisting separation. The detachment path was quite the contrary in the TDRDSTT–*RE* sample (see Figures 3f and 3g). In this case, the separation initiated from the N-terminus side, followed by D2 detachment, and finally completed by C-terminus T7 failure. The corresponding pull-out snapshots can be compared in Figure S10. The side-by-side separation movies of the *El* and *RE* sampling in the TDRDSTT peptide can be found in Movie S1. Overall, the peptides end

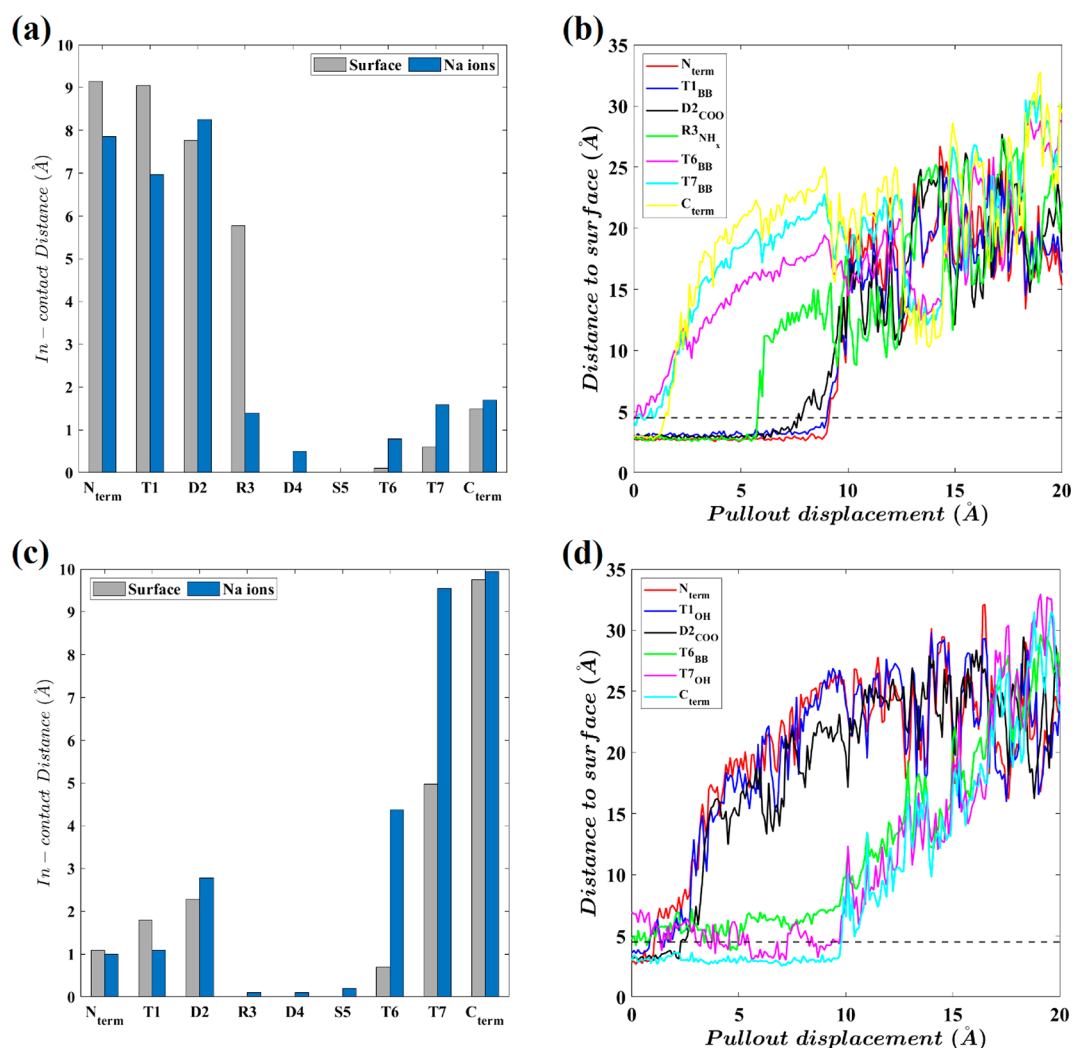


Figure 4. Maximum in-contact distance of each amino acid sequence of the TDRDSTT (coded as T1D2R3D4S5T6T7 in the figures) peptide from quartz and Na^+ counterions on the surface during the pull-out process of the equilibrated samples obtained by initial (a) elongated (*El*) and (c) replica-exchanged (*RE*) peptide on the surface. Evolution of the in-contact species distance during SMD, primarily initialized by (b) elongated (*El*) and (d) replica-exchanged (*RE*) peptides. The subscript BB denotes the backbone structure.

termini seemed to play a pivotal role in quartz–peptide interactions.

The interaction energy profiles also clarified two major insights. First, the interaction energy between Na^+ ions and the quartz surface was higher than that of Na^+ with negatively charged peptide residues. The Na^+ –peptide interaction energies became zero upon the full separation, suggesting that no ions would be dragged to the bulk water with the peptide. The claim is further confirmed by visually analyzing the SMD trajectory files. Second, in the T1D2R3D4S5T6T7 peptide, D4, S5, and T6 residues acted neutrally in the peptide–surface interactions. D4 contributed the most to the peptide–water interactions as the H-bond acceptor due to the $-\text{COO}^-$ moiety on its side group (see Figures 3d and 3h). The C-terminus formed a similar hydration shell with water molecules after being completely released from the surface influence.

The strongly binding residues versus the weaker binding were identified by close contact analysis. Figure 4 summarizes the in-contact distance of neighboring residues along with the evolution of pair residue–surface distance for the TDRDSTT peptide per *El* and *RE* samplings during SMD. The term “distance” in the “in-contact distance” refers to the displacement

of the peptide’s COM during the pull-out process. The residue and surface were assumed to be in close contact if the distance between heavy atoms of the residue fragment and the oxygen in the superficial SiOH/SiO^- layer was $<4.5 \text{ \AA}$ (i.e., border shown as a dashed horizontal line in Figure 4b,d). Comparing the maximum in-contact distance of amino acid sequences (Figure 4a,c) confirmed the different separation pathways, *a fortiori* for different adsorption modes, in the TDRDSTT–*El* and –*RE* samplings. In the *El* sampling, the amino acid sequences of the N-terminus side in (N-term)TDRDSTT(C-term) contributed more to the surface binding, whereas for the *RE* sampling, the binding responsibility was delegated to the C-terminus side.

The sequential detachment of the peptide fragments within the SMD process was captured by the distance analysis, as shown in Figure 4b,d. In *El* sampling (Figure 4b), the C-terminus was the first fragment detaching from the surface at $\sim 1.5 \text{ \AA}$. Upon the detachment, its distance increased with a steep slope and positioned at the farthest possible distance, greater than 20 \AA . The distance was proportional to the peptide length in its extended conformation. The guanidinium group in the arginine side chain was the second bounded residue to lose its connection to the surface at $\sim 5.8 \text{ \AA}$. The peptide separation was

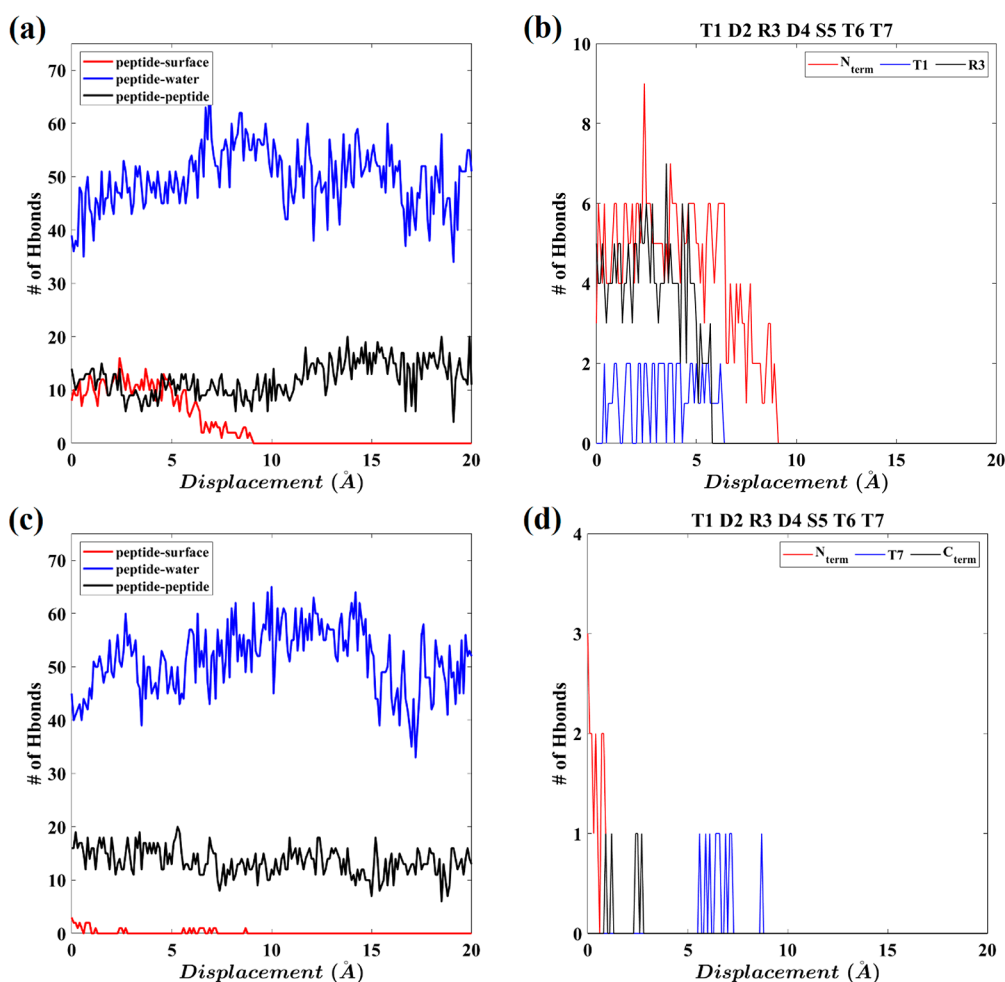


Figure 5. Evolution of the number of H-bonds in the overall system and per-species peptide–surface during the SMD process of the solvated TDRDSTT/quartz system, initially constructed by (a, b) elongated and (c, d) replica-exchanged peptide on the surface. The peptide has been coded as T1D2R3D4S5T6T7 in the figures.

completed by rupturing N-terminus T1 and D2 connections at ~ 9.1 Å.

Reviewing the close contact characteristics of the *RE* sampling (Figure 6d) showed the sequential detachment of the N-terminus T1, D2, and C-terminus T7 at ~ 1.1 , 2.3, and ~ 9.8 Å, respectively. The R3 residue, which contributed to *El* binding, did not play the same role in *RE* sampling. Hence, the fewer binding residues in the *RE* conformation was the main reason for the lower PMF values in *RE* samplings compared to the *El* ones in the TDRDSTT peptide (see Figure S8i).

The variation of the total and residue-specific number of H-bonds in the TDRDSTT–*El* and –*RE* systems during the SMD process is plotted in Figure 5. Based on the figure, the contribution of H-bonds completely differs in the two samplings. H-bonds appeared to have play a crucial role in peptide–quartz interactions in the *El* case, whereas H-bond contribution to the *RE* sampling was negligible (Figure 5a,c). There were ~ 10 H-bonds between the peptide and surface in the bound state per the *El* sampling (Figure 5a), while less than 2 H-bonds were found for the equilibrated *RE* system (see Figure 5c). The guanidinium group of arginine and ammonium of the N-terminus were the primary fragments associated with hydrogen bonding in the *El* sampling (Figure 5b). The hydroxyl group on the T1 side chain also formed a maximum of two intermittent H-bonds with the surface, which was ultimately

disrupted at ~ 6.4 Å. Before 5 Å, no changes in the average number of H-bonds were observed. This suggested that H-bonds were actively involved in keeping the peptide in contact with the surface. After pulling the peptide for 6.5 Å, more than two-thirds of the hydrogen bonds were broken. The results confirmed the simultaneous role of electrostatic and hydrogen bonding in the TDRDSTT–surface interactions.

For the *RE* sampling, as shown in Figure 5c, the number of intrapeptide H-bonds was almost twice the *El* case. Figure 5d further confirmed that the formation of the hydrogen bonding in *RE* sampling was occasional during the separation process. Therefore, electrostatic interactions are the dominant binding mechanism in the TDRDSTT–*RE* sampling. This observations here also indicated that the absence of hydrogen bonding was probably the main reason behind the lower PMF values for the *RE* samplings (see Figure S8i).

4.3.2. FTPDGAR Peptide: The Highest Affinity *El* Sampling.

The results for a system containing FTPDGAR peptide per *El* sampling are summarized in Figure 6. The interaction energy plots (Figure 6a–c) indicate that P3, G5, and A6 sequences of the FTPDGAR had a negligible contribution to the surface–peptide interactions. Previous studies revealed that the presence of proline in a sequence reduces the conformational flexibility of the peptide, which in turn can improve peptide–quartz affinities by keeping the extended conformation of the peptide.⁷³

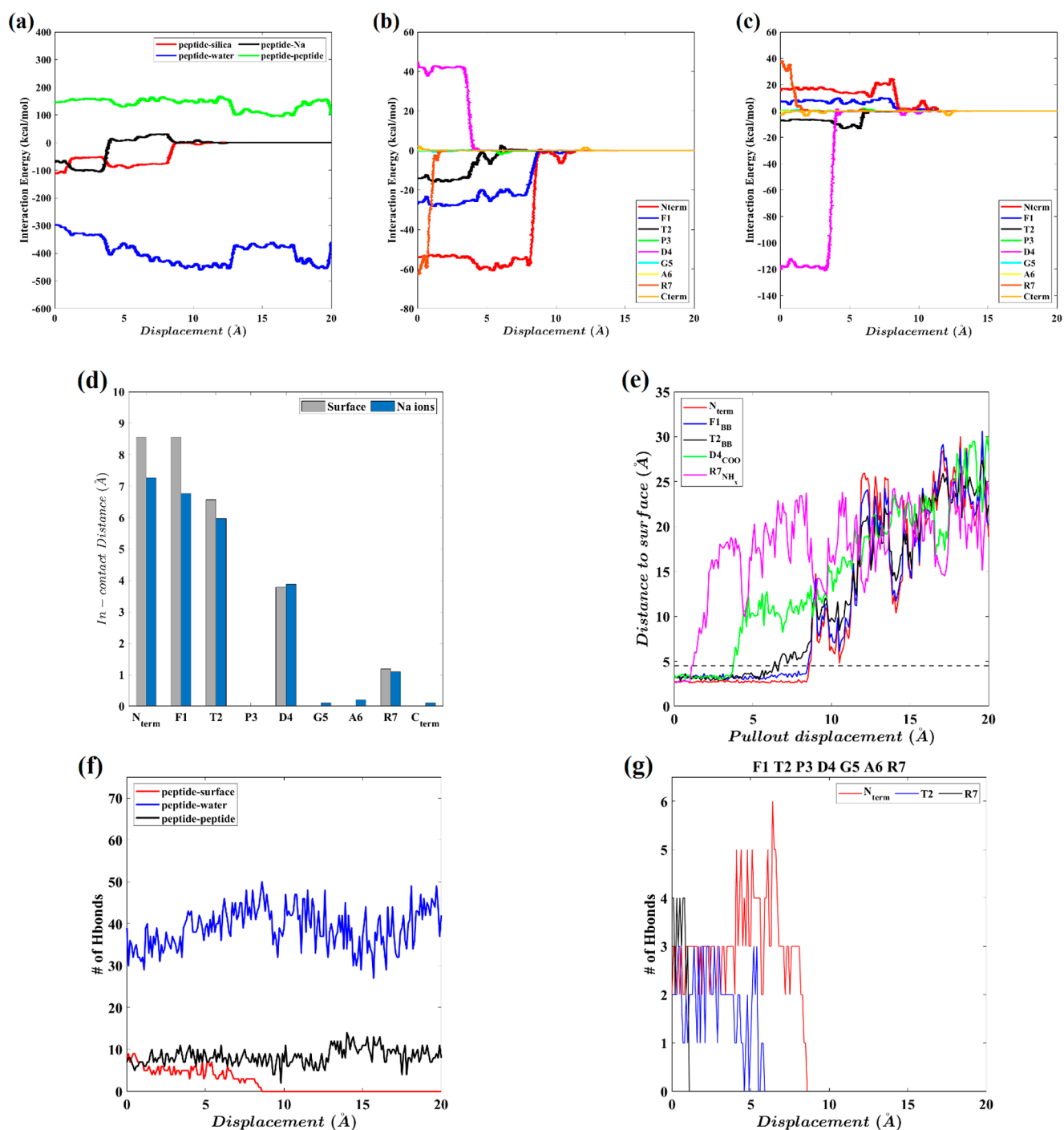


Figure 6. Variation of (a) overall interaction energies and sequence-specific (b) peptide-surface and (c) peptide-Na⁺ ions interactions, (d) maximum in-contact distance per amino acid sequence, (e) in-contact species distance, (f) the overall H-bond number, and (g) per-species H-bond number between peptide-surface during the SMD process of the solvated FTPDGAR/quartz system, initially constructed by the elongated (*El*) peptide on the surface. The subscript BB denotes the backbone structure.

Based on the results, the FTPDGAR peptide was primarily anchored to the surface by N-terminus F1, D4, and R7 residues. The arginine sequence, with an interaction energy of ~ -60 kcal/mol, was the highest at the bound state. The position of the arginine at the peptide's end tail has kept away the C-terminus from the surface, though no peptide-Na⁺ interactions have been recorded for the C-terminus end. The residue-specific interaction plots (Figures 6bc) also revealed that the T2 residue was attracted to both the quartz surface and the bounded Na⁺ counterions in the adsorption configuration. Threonine did not

play the same role when presented in the TDRDSTT combination. These observations suggest that although the individual identity of amino acids is important, their place in the sequence and the neighboring residues determine their effects on the nature of the interactions in the system.

Comparing the interaction energy of the FTPDGAR system with the TDRDSTT at the bound state further revealed that the FTPDGAR sum of interactions with the surface was higher than that of the peptide interactions with the surface-bound Na⁺ ions, which was a more active mechanism in TDRDSTT adsorption.

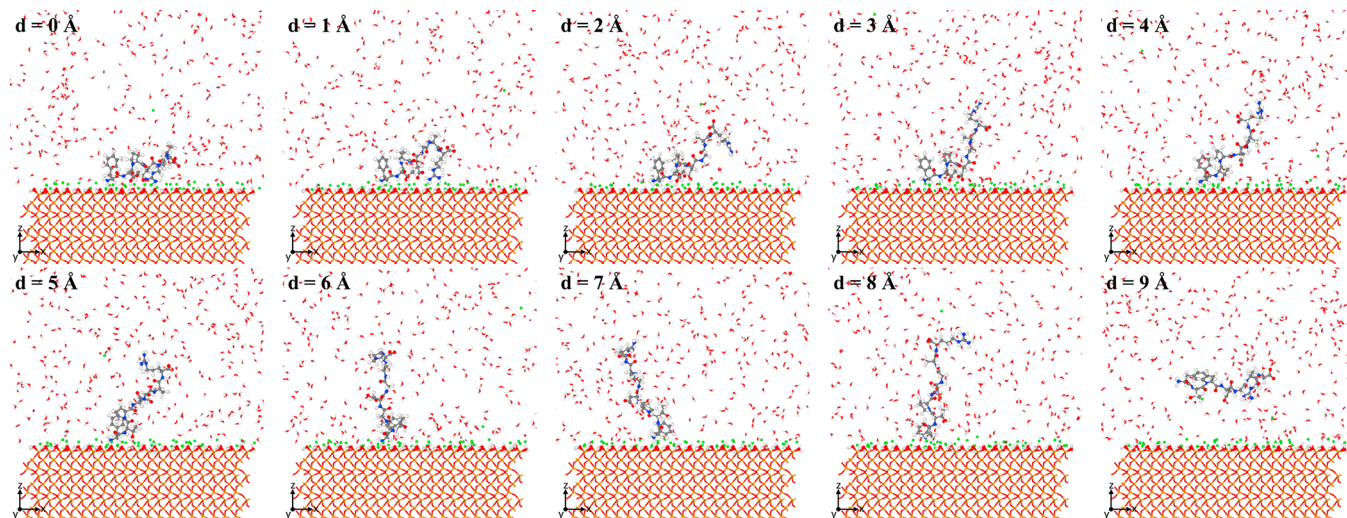


Figure 7. Snapshots correspond to the FTPDGAR conformations during the SMD simulations in the aqueous peptide/quartz system at pH = 9. The system was initially constructed by the elongated (*EL*) conformation (H \equiv white, C \equiv gray, N \equiv blue, O \equiv red, Si \equiv orange, and Na \equiv green). Note: the images are presented in the unwrap mode.

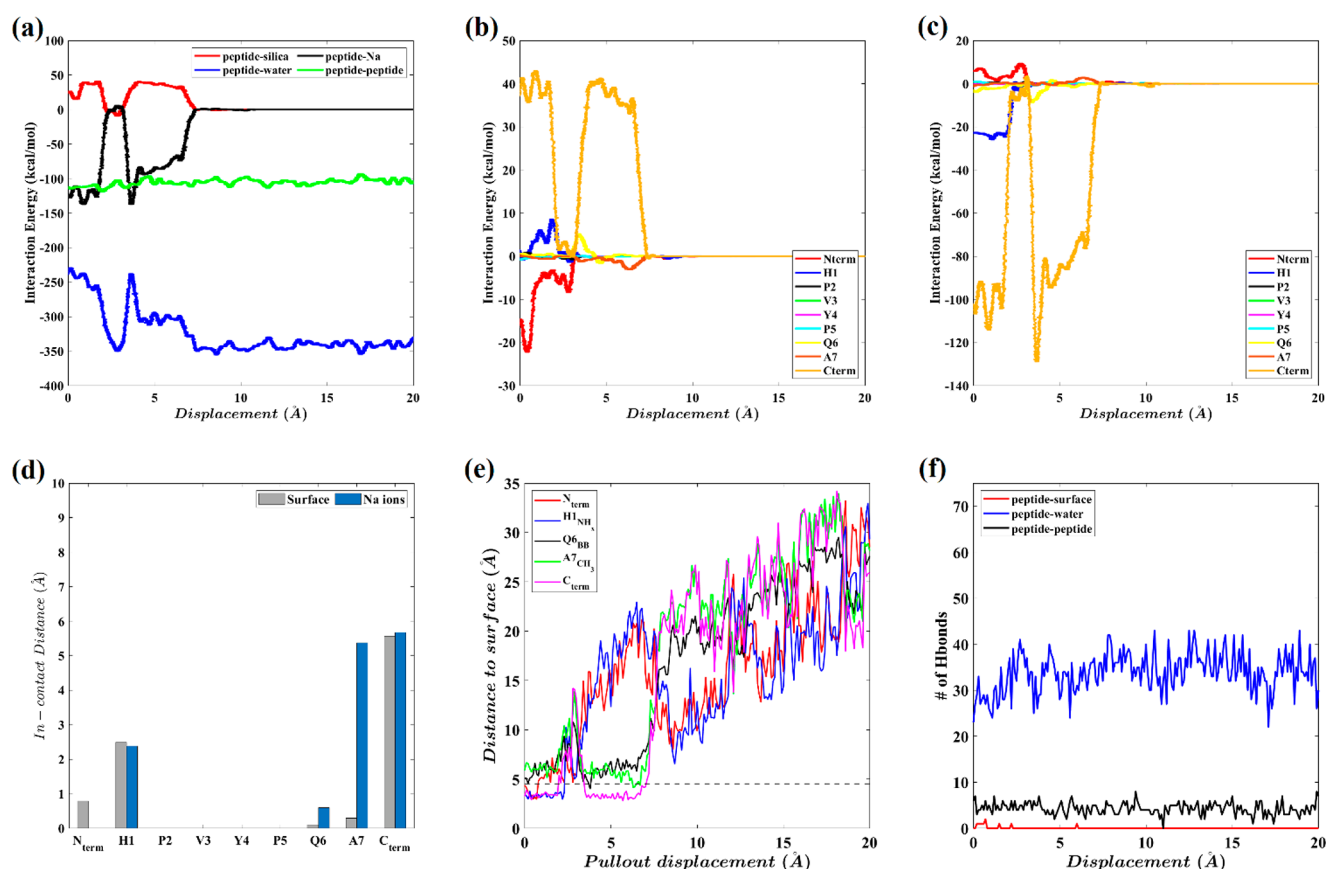


Figure 8. Variation of (a) overall interaction energies and the sequence-specific (b) peptide–surface and (c) peptide–Na⁺ ions interactions, (d) maximum in-contact distance per amino acid sequence, (e) in-contact species distance, and (f) the overall H-bond number during the SMD process of the solvated HPVYPQA/quartz system, initially constructed by the elongated (*EL*) peptide on the surface. The subscript BB denotes the backbone structure.

The peptide–peptide and peptide–water interactions in the FTPDGAR system were respectively less positive and negative than in the TDRDSTT system, in agreement with the former more hydrophobic residues in its chain combination.

The close contact analysis of the surface neighboring species and the respective hydrogen bond evolution for the FTPDGAR-

EL during the SMD process are shown in Figures 6d–g, while the separation trajectories are represented in Figure 7 and Movie S2. Based on the close contact results in Figure 6e, R7 was the first residue that lost its connection at ~ 1.2 Å. Before detachment, R7 had formed the maximum number of hydrogen bonds with the surface. D4 was the second residue that detached

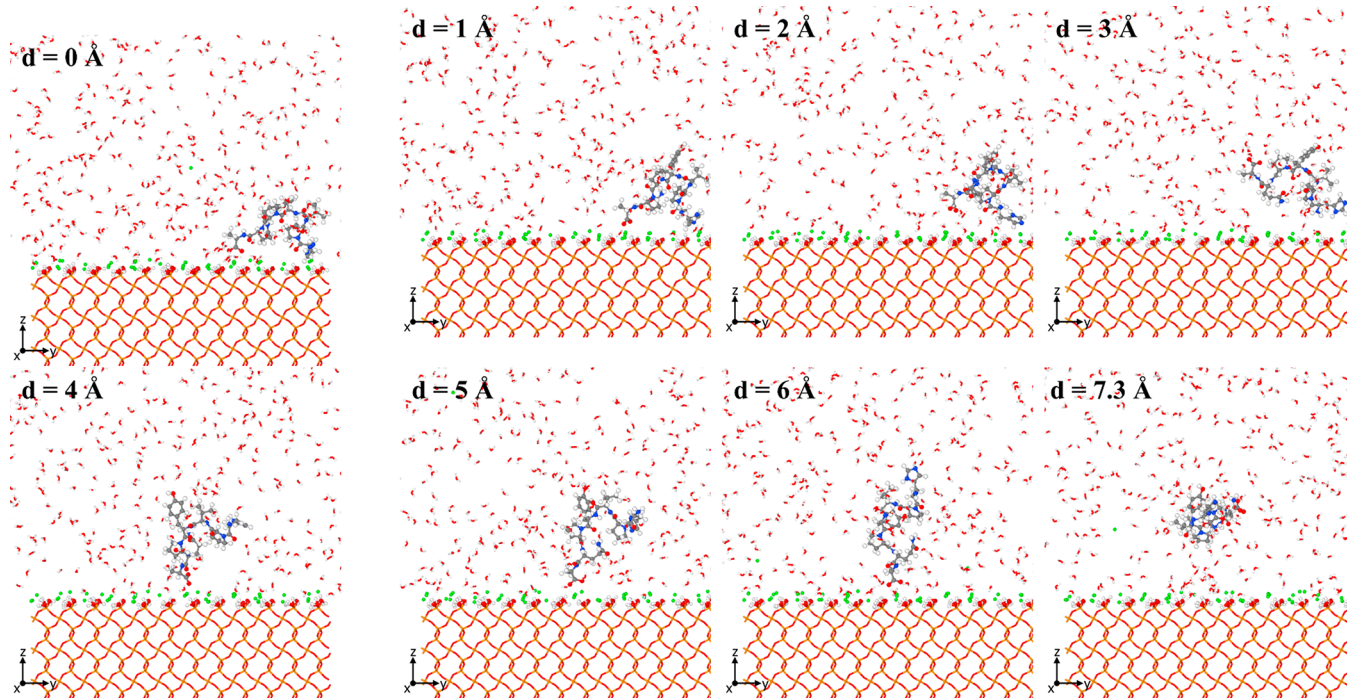


Figure 9. Snapshots correspond to the HPVYPQA conformations during the SMD simulations in the aqueous peptide/quartz system at pH = 9. The system was initially constructed by the elongated (*El*) conformation (H \equiv white, C \equiv gray, N \equiv blue, O \equiv red, Si \equiv orange, and Na \equiv green). Note: the images are presented in the unwrap mode.

from the surface at ~ 3.8 Å. Our analysis captured no H-bonds between the $-\text{COO}^-$ side chain of the D4 amino acid and the silanol group on the quartz surface. Therefore, the Na^+ bridging effect was probably the adsorption mechanism for D4 affinity toward the surface. The claim was further confirmed by the maximum in-contact distance of the D4 residue with the quartz surface and Na^+ ions (Figure 6d). T2 was shown to separate from the surface at ~ 6.7 Å. In the close contact analysis, the threonine side chain was not captured in the surface vicinity, and the hydrogen bonds were formed between the T2 backbone and the surface. The H-bond disruption of T2 residue led to an increase in the H-bond number of the N-terminus in the new conformation. The N-terminus F1 was finally ruptured at ~ 8.6 Å. The separation point of each residue was tantamount to an *inflection point* on the respective PMF–distance curves (Figure S8a).

It is noteworthy that the proximity of the phenylalanine (F1) backbone with the surface instead of the hydrophobic benzyl of its side chain proved that hydrophobic groups were not favorable to the negatively charged quartz surface at basic pHs (see Figure 6e). This is consistent with the previous prediction that the role of hydrophobic interactions would be significant at a lower degree of silica surface ionization.³⁴ Moreover, having two positively charged species at both ends of the FTPDGAR peptide seems to be a positive clue for stabilizing adsorption configurations on a negatively charged surface.

4.3.3. HPVYPQA Peptide: The Weakest-Bound Peptide Candidate. The adsorption/desorption characteristics of the HPVYPQA peptide, as the weakest binding candidate, during the pull-out process are summarized in Figure 8. As mentioned earlier, the RE sampling procedure for the peptide came up with unbound configurations within the equilibration time scale. Consequently, our observations here are limited to the *El* sampling only. On the basis of the overall interaction energies shown in Figure 8a, the intrapeptide interactions were negative,

indicating attractive intramolecular forces within the peptide chain. The negative intrapeptide interactions alluded to the higher tendency of the peptide to fold onto itself in the aqueous environment. The peptide–water interactions in the HPVYPQA system were lower than those of the strongest binding peptides (Figures 3a and 6a), further confirming that the HPVYPQA peptide tends to minimize the interaction of its hydrophobic residues (i.e., V3, Y4, and A7) with water. As evident in Figures 8b and 8c, C-terminus and N-terminus H1 were the only residues latching HPVYPQA to the surface. The interaction energy captured for the N-terminus species in HPVYPQA was less than one-third of the values recorded for the TDRDSTT and FTPDGAR peptides. The P2, V3, Y4, P5, and even the A7 residue at the end tail position had almost no contributions to the surface binding.

Based on the close contact analysis in Figures 8d and 8e, the N-terminus was the initial species that lost contact with the surface at ~ 0.8 Å. After that, due to the geometrical restriction, the N-terminus remained in the vicinity of the surface until the detachment of H1 residue at ~ 2.4 Å. The close contact analysis in Figure 8e suggested a significant reorganization of HPVYPQA peptide within 2–3.5 Å of the pulling by the temporary detachment of the C-terminus from the surface. The snapshots in Figure 9 and Movie S3 had instructively captured the intermediate conformations. Within the interval, the peptide remained loosely bound to the surface with the weak surface–peptide interactions through the N-terminus H1 residue. Alanine placement near the end C-terminal with its hydrophobic side group was probably the main reason behind the observed phenomenon. After the reorganization, the C-terminus was reattached to the surface and solely kept the peptide in contact with the surface upon its ultimate disruption at ~ 7.2 Å.

The evolution of the total number of H-bonds in the HPVYPQA system is presented in Figure 8f. As evident, hydrogen bonding had thereby trivial contribution to surface–

peptide interactions. The N-terminus and histidine side chain were involved in the observed initial partial intermittent H-bonds. Therefore, one can conclude that electrostatic and vdW interactions are the only binding mechanism in the HPVYPQA systems. Our analysis (not shown here) further reveals that Q6 residue formed the highest number of H-bonds with water molecules at the bound state. After the full separation, N-terminus and Q6 residues built more than 70% of the H-bonds networks in peptide–water interactions.

5. CONCLUSION

In this work, we devised a sequential scheme to perform atomistic simulations of adsorption and binding characteristics of peptides on inorganic surfaces, combining classical MD, replica exchange MD (REMD), and steered MD (SMD). Within the procedure, the peptide sequences suggested by phage display screening were initially sampled within the REMD framework under the implicit water model, continued with explicit water introduction, equilibrated by classical MD, and finally characterized by SMD simulations. The introduced simulation method has several advantages over the common classical approaches. First, employing REMD would boost sampling diversity more genuinely than solely using classical MD theory. Second, the sequential addition of system components would facilitate the equilibration process, whereas a high level of convergence in equilibrium structure and energies was reached. Third, applying SMD simulations would substantively discriminate between the strongest and weakest binding peptides and provide a detailed atomistic description of the unbinding mechanism by clarifying the active from inactive compounds.

The procedure mentioned above was employed to study the adsorption of ten 7-mer peptides, experimentally identified by phage display, on the crystalline quartz surface at pH = 9. The quartz slab contains silanol and siloxide groups on the exposed surface layer in a basic environment, leading to an ultimate negatively charged substrate. Our observations revealed that the mechanism and extent of binding were mainly controlled by the local surface environment, the identity of amino acids, the peptide's composition, and the placement positions of residues in the sequence. Generally, at pH 9, the affinity of amino acids followed the trend of positively charged > negatively charged >> uncharged toward the quartz surface. The adsorption of N-termini and positively charged amino acid residues was more favorable due to the simultaneous action of polar electrostatic interactions (i.e., mainly through ion-pairing) and hydrogen bonding. The C-termini and negatively charged residues mainly bound the surface with an electrostatic bridging with the surface-bound Na⁺ counterions at pH = 9. The uncharged residues (except the hydrophobic species) formed weak intermittent contact with the surface through van der Waals and weak hydrogen bond interactions.

Putting aside the N- and C-termini, R⁺ and K⁺ residues were identified as the most potent binders to the quartz surface in the peptide sequence. The contribution of D⁻ and E⁻ residues was also significant due to the prevailing concentration of surface-bound Na⁺ ions at pH 9. The adsorption mechanism of weaker-binding peptides involved a considerable decline in hydrogen bonding. In particular, our results revealed that the peptides with a combined association of positively and negatively charged residues in the sequence showed the highest affinity to the quartz surface at pH 9. As an extreme, the incorporation of R⁺ and D⁻ in the peptide sequence resulted in the most notable contributions

toward surface binding. The proximity of positively charged and negatively charged residues in the sequence seemed to be the key point in designing robust selective peptides toward the quartz surface. However, assessments of more peptides are needed. One should also be aware of the importance of intrapeptide interaction in peptide–surface interactions. Our results suggest that repulsive intrapeptide interactions (as identified by the positive peptide–peptide interactions), in accordance with the occurrence of more stretched conformations, are favorable for strong peptide–quartz binding.

Overall, the proposed approach enables a better description of the binding process of peptides to quartz by increasing the system resolution to the atomic level and suggests that the adsorption mechanism is tunable by manipulating peptide sequences. Furthermore, the simulations confirm that the recent developments in computational methods present a unique opportunity for rational reagent design approaches.

■ ASSOCIATED CONTENT

SI Supporting Information

The Supporting Information is available free of charge at <https://pubs.acs.org/doi/10.1021/acsami.3c01275>.

Information on the molecular models of peptides, quartz slab, and complex model construction (Figure S1–S3); sample monitoring of replica's temperature, COM, and radius of gyration during the initial REMD sampling in an implicit water model (Figure S4) and postprocessing on the final 5 ns of the REMD simulation by focusing on calculating interaction energies (Figure S5) and hydrogen bonding (Figure S6); snapshots of the equilibrated water–peptide–quartz systems (Figure S7); detailed PMF profiles of the peptides separation from quartz surface obtained by SMD simulations (Figure S8); SMD trajectory snapshots for the TDRDSTT peptide through *El* (Figure S9) and *RE* (Figure S10) samplings (PDF)

Movie S1: separation of the TDRDSTT peptide from the quartz surface obtained by SMD simulation (MP4)

Movie S2: separation of the FTPDGAR peptide from the quartz surface obtained by SMD simulation (MP4)

Movie S3: separation of the HPVYPQA peptide from the quartz surface obtained by SMD simulation (MP4)

■ AUTHOR INFORMATION

Corresponding Authors

Faïçal Larachi – Department of Chemical Engineering, Université Laval, Québec, Québec G1V 0A6, Canada; orcid.org/0000-0002-0127-4738; Email: faical.larachi@gch.ulaval.ca

Patrick Lagüe – PROTEO, The Quebec Network for Research on Protein Function, Engineering, and Applications, Québec, Québec G1V 0A6, Canada; IBIS, Institut de biologie intégrative et des systèmes, Québec, Québec G1V 0A6, Canada; Department of Biochemistry, Microbiology and Bioinformatics, Université Laval, Québec, Québec G1V 0A6, Canada; orcid.org/0000-0002-5236-4979; Email: patrick.lague@bcm.ulaval.ca

Authors

Abolfazl Alizadeh Sahraei – Department of Chemical Engineering, Université Laval, Québec, Québec G1V 0A6, Canada; orcid.org/0000-0001-7103-7001

Barbara Mejia Bohorquez – Department of Chemical Engineering, Université Laval, Québec, Québec G1V 0A6, Canada; PROTEO, The Quebec Network for Research on Protein Function, Engineering, and Applications, Québec, Québec G1V 0A6, Canada

Denise Tremblay – PROTEO, The Quebec Network for Research on Protein Function, Engineering, and Applications, Québec, Québec G1V 0A6, Canada; IBIS, Institut de biologie intégrative et des systèmes, Québec, Québec G1V 0A6, Canada; Department of Biochemistry, Microbiology and Bioinformatics, Université Laval, Québec, Québec G1V 0A6, Canada

Sylvain Moineau – PROTEO, The Quebec Network for Research on Protein Function, Engineering, and Applications, Québec, Québec G1V 0A6, Canada; IBIS, Institut de biologie intégrative et des systèmes, Québec, Québec G1V 0A6, Canada; Department of Biochemistry, Microbiology and Bioinformatics, Université Laval, Québec, Québec G1V 0A6, Canada;

orcid.org/0000-0002-2832-5101

Alain Garnier – Department of Chemical Engineering, Université Laval, Québec, Québec G1V 0A6, Canada; PROTEO, The Quebec Network for Research on Protein Function, Engineering, and Applications, Québec, Québec G1V 0A6, Canada

Complete contact information is available at:
<https://pubs.acs.org/10.1021/acsami.3c01275>

Notes

The authors declare no competing financial interest.

ACKNOWLEDGMENTS

The authors gratefully acknowledge the Natural Sciences and Engineering Research Council of Canada for their financial support. We are also indebted to Compute Canada for the HPC platform, without which the present MD simulations would not have been possible. We also acknowledge MITACS, COREM, CRIBIQ, Agnico Eagle, and Chemiqa/Flottec for providing financial support. S.M. holds the Canada Research Chair in Bacteriophages.

REFERENCES

- (1) Werner, T. T.; Bebbington, A.; Gregory, G. Assessing Impacts of Mining: Recent Contributions from GIS and Remote Sensing. *Extractive Industries and Society* **2019**, *6* (3), 993–1012.
- (2) Xu, D.-M.; Zhan, C.-L.; Liu, H.-X.; Lin, H.-Z. A Critical Review on Environmental Implications, Recycling Strategies, and Ecological Remediation for Mine Tailings. *Environ. Sci. Pollut. Res.* **2019**, *26* (35), 35657–35669.
- (3) Kyzas, G. Z.; Matis, K. A. The Flotation Process Can Go Green. *Processes* **2019**, *7* (3), 138.
- (4) Setiawan, W. K.; Chiang, K.-Y. Silica Applied as Mixed Matrix Membrane Inorganic Filler for Gas Separation: A Review. *Sustainable Environment Research* **2019**, *29* (1), 32.
- (5) Si, Y.; Li, J.; Cui, B.; Tang, D.; Yang, L.; Murugadoss, V.; Maganti, S.; Huang, M.; Guo, Z. Janus Phenol–Formaldehyde Resin and Periodic Mesoporous Organic Silica Nano-adsorbent for the Removal of Heavy Metal Ions and Organic Dyes from Polluted Water. *Advanced Composites and Hybrid Materials* **2022**, *5* (2), 1180–1195.
- (6) Croissant, J. G.; Butler, K. S.; Zink, J. I.; Brinker, C. J. Synthetic Amorphous Silica Nanoparticles: Toxicity, Biomedical and Environmental Implications. *Nat. Rev. Mater.* **2020**, *5* (12), 886–909.
- (7) Manzano, M.; Vallet-Regí, M. Mesoporous Silica Nanoparticles for Drug Delivery. *Adv. Funct. Mater.* **2020**, *30* (2), 1902634.
- (8) Ekeoma, B. C.; Yusuf, M.; Johari, K.; Abdullah, B. Mesoporous Silica Supported Ni-Based Catalysts for Methane Dry Reforming: A

Review Of Recent Studies. *Int. J. Hydrogen Energy* **2022**, *47* (98), 41596–41620.

(9) Boroun, S.; Alizadeh Sahraei, A.; Mokarizadeh, A. H.; Alamdari, H.; Fontaine, F.-G.; Larachi, F. Insights into the Solubility of Carbon Dioxide in Grafted Mesoporous Silica for the Catalytic Synthesis of Cyclic Carbonates by Nanoconfinement. *ACS Appl. Mater. Interfaces* **2021**, *13* (23), 27019–27028.

(10) Raju, N. A.; Prasad, D.; Srinivasappa, P. M.; Biradar, A. V.; Gholap, S. S.; Samal, A. K.; Nagaraja, B. M.; Jadhav, A. H. Recent Developments in State-of-the-art Silica-modified Catalysts for the Fixation of CO₂ in Epoxides to Form Organic Carbonates. *Sustainable Energy & Fuels* **2022**, *6* (5), 1198–1248.

(11) Xie, P.; Shi, Z.; Feng, M.; Sun, K.; Liu, Y.; Yan, K.; Liu, C.; Moussa, T. A. A.; Huang, M.; Meng, S.; Liang, G.; Hou, H.; Fan, R.; Guo, Z. Recent Advances in Radio-Frequency Negative Dielectric Metamaterials by Designing Heterogeneous Composites. *Advanced Composites and Hybrid Materials* **2022**, *5* (2), 679–695.

(12) Zhang, Z.; Liu, M.; Ibrahim, M. M.; Wu, H.; Wu, Y.; Li, Y.; Mersal, G. A. M.; El Azab, I. H.; El-Bahy, S. M.; Huang, M.; Jiang, Y.; Liang, G.; Xie, P.; Liu, C. Flexible Polystyrene/Graphene Composites with Epsilon-near-zero Properties. *Advanced Composites and Hybrid Materials* **2022**, *5* (2), 1054–1066.

(13) Guzel Kaya, G.; Deveci, H. Synergistic Effects of Silica Aerogels/Xerogels on Properties of Polymer Composites: A Review. *J. Ind. Eng. Chem.* **2020**, *89*, 13–27.

(14) Chen, Z.; Huang, Y. Preparation and Performance of Fumed Silica-Stabilized Epoxy Resin Pickering Emulsion for Basalt Fiber-Sizing Agents. *Advanced Composites and Hybrid Materials* **2021**, *4* (4), 1205–1214.

(15) Fuerstenau, M. C.; Jameson, G. J.; Yoon, R. H. *Froth Flotation: A Century of Innovation*; Society for Mining, Metallurgy, and Exploration: 2007.

(16) Zhang, X.; Gu, X.; Han, Y.; Parra-Álvarez, N.; Claremboux, V.; Kawatra, S. K. Flotation of Iron Ores: A Review. *Mineral Processing and Extractive Metallurgy Review* **2021**, *42* (3), 184–212.

(17) Fan, G.; Wang, L.; Cao, Y.; Li, C. Collecting Agent–mineral Interactions in the Reverse Flotation of Iron Ore: A Brief Review. *Minerals* **2020**, *10* (8), 681.

(18) Johnson, D. B. Biomining—biotechnologies for Extracting and Recovering Metals from Ores and Waste Materials. *Curr. Opin. Biotechnol.* **2014**, *30*, 24–31.

(19) Tremblay-Bouliane, K.; Tremblay, D.; Moineau, S.; Gaillet, B.; Garnier, A.; Olsen, C. Screening Peptide-ore Interactions with a Phage Display Library for Bioflotation Application. *CIM Journal* **2016**, *7*, 178–184.

(20) Ozaki, M.; Sakashita, S.; Hamada, Y.; Usui, K. Peptides for Silica Precipitation: Amino Acid Sequences for Directing Mineralization. *Protein & Peptide Letters* **2018**, *25* (1), 15–24.

(21) Azizi, D.; Larachi, F.; Garnier, A.; Lagüe, P.; Levasseur, B. Sorption of Aqueous Amino Acid Species on Sulphidic Mineral Surfaces—DFT Study And Insights on Biosourced-reagent Mineral Flotation. *Canadian Journal of Chemical Engineering* **2021**, *99* (8), 1758–1779.

(22) Alizadeh Sahraei, A.; Larachi, F. Chemical Transformation and Dissociation of Amino Acids on Metal Sulfide Surface: Insights from DFT into the Effect of Surface Vacancies on Alanine-sphalerite System. *Appl. Surf. Sci.* **2021**, *540*, 148304.

(23) Alizadeh Sahraei, A.; Larachi, F. Electronic Simulations of Alanine and Water Co-adsorption over Defect-Free and Sulfur-Depleted Sphalerite Surfaces. *Appl. Surf. Sci.* **2022**, *576*, 151899.

(24) Pande, J.; Szewczyk, M. M.; Grover, A. K. Phage display: Concept, Innovations, Applications and Future. *Biotechnology Advances* **2010**, *28* (6), 849–858.

(25) Xu, P.; Ghosh, S.; Gul, A. R.; Bhamore, J. R.; Park, J. P.; Park, T. J. Screening of Specific Binding Peptides Using Phage-Display Techniques and Their Biosensing Applications. *TrAC Trends in Analytical Chemistry* **2021**, *137*, 116229.

(26) Smith, G. P.; Petrenko, V. A. Phage Display. *Chem. Rev.* **1997**, *97* (2), 391–410.

- (27) Derda, R.; Tang, S. K. Y.; Li, S. C.; Ng, S.; Matochko, W.; Jafari, M. R. Diversity of Phage-displayed Libraries of Peptides During Panning and Amplification. *Molecules* **2011**, *16* (2), 1776–1803.
- (28) 't Hoen, P. A. C.; Jirka, S. M. G.; ten Broeke, B. R.; Schultes, E. A.; Aguilera, B.; Pang, K. H.; Heemskerck, H.; Aartsma-Rus, A.; van Ommen, G. J.; den Dunnen, J. T. Phage Display Screening Without Repetitious Selection Rounds. *Anal. Biochem.* **2012**, *421* (2), 622–631.
- (29) He, B.; Jiang, L.; Duan, Y.; Chai, G.; Fang, Y.; Kang, J.; Yu, M.; Li, N.; Tang, Z.; Yao, P.; Wu, P.; Derda, R.; Huang, J. Biopanning Data Bank 2018: Hugging Next Generation Phage Display. *Database* **2018**, *2018*, bay032.
- (30) He, B.; Chen, H.; Li, N.; Huang, J. SAROTUP: a Suite of Tools for Finding Potential Target-unrelated Peptides from Phage Display Data. *International Journal of Biological Sciences* **2019**, *15* (7), 1452–1459.
- (31) Notman, R.; Oren, E. E.; Tamerler, C.; Sarikaya, M.; Samudrala, R.; Walsh, T. R. Solution Study of Engineered Quartz Binding Peptides Using Replica Exchange Molecular Dynamics. *Biomacromolecules* **2010**, *11* (12), 3266–3274.
- (32) Patwardhan, S. V.; Emami, F. S.; Berry, R. J.; Jones, S. E.; Naik, R. R.; Deschaume, O.; Heinz, H.; Perry, C. C. Chemistry of Aqueous Silica Nanoparticle Surfaces and the Mechanism of Selective Peptide Adsorption. *J. Am. Chem. Soc.* **2012**, *134* (14), 6244–6256.
- (33) Emami, F. S.; Puddu, V.; Berry, R. J.; Varshney, V.; Patwardhan, S. V.; Perry, C. C.; Heinz, H. Force Field and a Surface Model Database for Silica to Simulate Interfacial Properties in Atomic Resolution. *Chem. Mater.* **2014**, *26* (8), 2647–2658.
- (34) Emami, F. S.; Puddu, V.; Berry, R. J.; Varshney, V.; Patwardhan, S. V.; Perry, C. C.; Heinz, H. Prediction of Specific Biomolecule Adsorption on Silica Surfaces as a Function of pH and Particle Size. *Chem. Mater.* **2014**, *26* (19), 5725–5734.
- (35) Ramakrishnan, S. K.; Martin, M.; Cloitre, T.; Firlej, L.; Gergely, C. Molecular Mechanism of Selective Binding of Peptides to Silicon Surface. *J. Chem. Inf. Model.* **2014**, *54* (7), 2117–2126.
- (36) Puddu, V.; Perry, C. C. Interactions at the Silica–Peptide Interface: The Influence of Particle Size and Surface Functionality. *Langmuir* **2014**, *30* (1), 227–233.
- (37) Ramakrishnan, S. K.; Jebors, S.; Martin, M.; Cloitre, T.; Agarwal, V.; Mehdi, A.; Martinez, J.; Subra, G.; Gergely, C. Engineered Adhesion Peptides for Improved Silicon Adsorption. *Langmuir* **2015**, *31* (43), 11868–11874.
- (38) Costa, D.; Savio, L.; Pradier, C. M. Adsorption of Amino Acids and Peptides on Metal and Oxide Surfaces in Water Environment: A Synthetic and Prospective Review. *J. Phys. Chem. B* **2016**, *120* (29), 7039–7052.
- (39) Heinz, H.; Ramezani-Dakheel, H. Simulations of Inorganic–Bioorganic Interfaces to Discover New Materials: Insights, Comparisons to Experiment, Challenges, and Opportunities. *Chem. Soc. Rev.* **2016**, *45* (2), 412–448.
- (40) Ramakrishnan, S. K.; Zhu, J.; Gergely, C. Organic–inorganic Interface Simulation for New Material Discoveries. *WIREs Computational Molecular Science* **2017**, *7* (1), No. e1277.
- (41) Choi, Y. K.; Kern, N. R.; Kim, S.; Kanhaiya, K.; Afshar, Y.; Jeon, S. H.; Jo, S.; Brooks, B. R.; Lee, J.; Tadmor, E. B.; Heinz, H.; Im, W. CHARMM-GUI Nanomaterial Modeler for Modeling and Simulation of Nanomaterial Systems. *J. Chem. Theory Comput.* **2022**, *18* (1), 479–493.
- (42) Geng, H.; Chen, F.; Ye, J.; Jiang, F. Applications of Molecular Dynamics Simulation in Structure Prediction of Peptides and Proteins. *Computational and Structural Biotechnology Journal* **2019**, *17*, 1162–1170.
- (43) Brancolini, G.; Bellucci, L.; Maschio, M. C.; Di Felice, R.; Corni, S. The Interaction of Peptides and Proteins with Nanostructures Surfaces: A Challenge for Nanoscience. *Curr. Opin. Colloid Interface Sci.* **2019**, *41*, 86–94.
- (44) Earl, D. J.; Deem, M. W. Parallel Tempering: Theory, Applications, and New Perspectives. *Phys. Chem. Chem. Phys.* **2005**, *7* (23), 3910–3916.
- (45) Barducci, A.; Bonomi, M.; Parrinello, M. Metadynamics. *WIREs Computational Molecular Science* **2011**, *1* (5), 826–843.
- (46) Sampath, J.; Pfandner, J. Amphiphilic Peptide Binding on Crystalline vs. Amorphous Silica from Molecular Dynamics Simulations. *Mol. Phys.* **2019**, *117* (23–24), 3642–3650.
- (47) Wang, L.; Sun, W.; Liu, R.-q. Mechanism of Separating Muscovite and Quartz by Flotation. *Journal of Central South University* **2014**, *21* (9), 3596–3602.
- (48) Huang, Z.; Zhong, H.; Wang, S.; Xia, L.; Zou, W.; Liu, G. Investigations on Reverse Cationic Flotation of Iron Ore by Using a Gemini Surfactant: Ethane-1,2-Bis(Dimethyl-Dodecyl-Ammonium Bromide). *Chem. Eng. J.* **2014**, *257*, 218–228.
- (49) Liu, A.; Fan, J.-c.; Fan, M.-q. Quantum Chemical Calculations and Molecular Dynamics Simulations of Amine Collector Adsorption on Quartz (0 0 1) Surface in the Aqueous Solution. *Int. J. Miner. Process.* **2015**, *134*, 1–10.
- (50) Li, L.; Hao, H.; Yuan, Z.; Liu, J. Molecular Dynamics Simulation of Siderite-Hematite-Quartz Flotation with Sodium Oleate. *Appl. Surf. Sci.* **2017**, *419*, 557–563.
- (51) Veloso, C. H.; Filippov, L. O.; Filippova, I. V.; Ouvrard, S.; Araujo, A. C. Investigation of the Interaction Mechanism of Depressants in the Reverse Cationic Flotation of Complex Iron Ores. *Minerals Engineering* **2018**, *125*, 133–139.
- (52) Huang, J.; Ru, B.; Zhu, P.; Nie, F.; Yang, J.; Wang, X.; Dai, P.; Lin, H.; Guo, F.-B.; Rao, N. MimoDB 2.0: A Mimotope Database and Beyond. *Nucleic Acids Res.* **2012**, *40* (D1), D271–D277.
- (53) Patel, J. S.; Berteotti, A.; Ronsisvalle, S.; Rocchia, W.; Cavalli, A. Steered Molecular Dynamics Simulations for Studying Protein–Ligand Interaction in Cyclin-Dependent Kinase S. *J. Chem. Inf. Model.* **2014**, *54* (2), 470–480.
- (54) Hoff, S. E.; Liu, J.; Heinz, H. Binding Mechanism and Binding Free Energy of Amino Acids and Citrate to Hydroxyapatite Surfaces as a Function of Crystallographic Facet, Ph, and Electrolytes. *J. Colloid Interface Sci.* **2022**, *605*, 685–700.
- (55) New England Biolabs. Ph.D. Phage Display Libraries. Instruction Manual. Preprint at (2014).
- (56) Matochko, W. L.; Chu, K.; Jin, B.; Lee, S. W.; Whitesides, G. M.; Derda, R. Deep Sequencing Analysis of Phage Libraries Using Illumina Platform. *Methods* **2012**, *58* (1), 47–55.
- (57) Illumina Support. 16s Metagenomic Sequencing Library Preparation; Illumina, San Diego, CA, 2013. https://support.illumina.com/downloads/16s_metagenomic_sequencing_library_preparation.html (accessed 2013-11-27).
- (58) Osorio, D.; Rondon-Villarreal, P.; Torres, R. Peptides: A Package for Data Mining of Antimicrobial Peptides. *R Journal* **2015**, *7* (1), 4–14.
- (59) Avogadro: An Open-source Molecular Builder and Visualization Tool, ver. 1.2.0 (<http://avogadro.cc/>).
- (60) Hanwell, M. D.; Curtis, D. E.; Lonie, D. C.; Vandermeersch, T.; Zurek, E.; Hutchison, G. R. Avogadro: An Advanced Semantic Chemical Editor, Visualization, and Analysis Platform. *Journal of Cheminformatics* **2012**, *4* (1), 17.
- (61) Patriksson, A.; van der Spoel, D. A Temperature Predictor for Parallel Tempering Simulations. *Phys. Chem. Chem. Phys.* **2008**, *10* (15), 2073–2077.
- (62) Kofke, D. A. On the Acceptance Probability of Replica-Exchange Monte Carlo Trials. *J. Chem. Phys.* **2002**, *117* (15), 6911–6914.
- (63) Huang, J.; Rauscher, S.; Nawrocki, G.; Ran, T.; Feig, M.; de Groot, B. L.; Grubmüller, H.; MacKerell, A. D. CHARMM36m: An Improved Force Field for Folded and Intrinsically Disordered Proteins. *Nat. Methods* **2017**, *14* (1), 71–73.
- (64) Boonstra, S.; Onck, P. R.; van der Giessen, E. CHARMM TIP3P Water Model Suppresses Peptide Folding by Solvating the Unfolded State. *J. Phys. Chem. B* **2016**, *120* (15), 3692–3698.
- (65) Thompson, A. P.; Aktulga, H. M.; Berger, R.; Bolintineanu, D. S.; Brown, W. M.; Crozier, P. S.; in 't Veld, P. J.; Kohlmeyer, A.; Moore, S. G.; Nguyen, T. D.; Shan, R.; Stevens, M. J.; Tranchida, J.; Trott, C.; Plimpton, S. J. LAMMPS - A Flexible Simulation Tool for Particle-Based Materials Modeling at the Atomic, Meso, and Continuum Scales. *Comput. Phys. Commun.* **2022**, *271*, 108171.

(66) Stukowski, A. Visualization and Analysis of Atomistic Simulation Data with OVITO—The Open Visualization Tool. *Modell. Simul. Mater. Sci. Eng.* **2010**, *18* (1), 015012.

(67) Ryckaert, J.-P.; Ciccotti, G.; Berendsen, H. J. C. Numerical Integration of the Cartesian Equations of Motion of a System with Constraints: Molecular Dynamics of N-alkanes. *J. Comput. Phys.* **1977**, *23* (3), 327–341.

(68) Chen, S.-H.; Singer, S. J. Molecular Dynamics Study of the Electric Double Layer and Nonlinear Spectroscopy at the Amorphous Silica–Water Interface. *J. Phys. Chem. B* **2019**, *123* (29), 6364–6384.

(69) Jarzynski, C. Nonequilibrium Equality for Free Energy Differences. *Phys. Rev. Lett.* **1997**, *78* (14), 2690–2693.

(70) Park, S.; Schulten, K. Calculating Potentials of Mean Force from Steered Molecular Dynamics Simulations. *J. Chem. Phys.* **2004**, *120* (13), 5946–5961.

(71) Estephan, E.; Dao, J.; Saab, M.-B.; Panayotov, I.; Martin, M.; Larroque, C.; Gergely, C.; Cuisinier, F. J. G.; Levallois, B. SVSVGMPKSPRP: A Broad Range Adhesion Peptide. *Biomedizinische Technik/Biomedical Engineering* **2012**, *57* (6), 481–489.

(72) Kolb, G.; Boiziau, C. Selection by Phage Display of Peptides Targeting the HIV-1 TAR Element. *RNA Biology* **2005**, *2* (1), 28–33.

(73) Oren, E. E.; Tamerler, C.; Sahin, D.; Hnilova, M.; Seker, U. O. S.; Sarikaya, M.; Samudrala, R. A Novel Knowledge-Based Approach to Design Inorganic-Binding Peptides. *Bioinformatics* **2007**, *23* (21), 2816–2822.